

# VMonarch: Efficient Video Diffusion Transformers with Structured Attention

Cheng Liang<sup>1,3\*</sup>, Haoxian Chen<sup>1</sup>, Liang Hou<sup>3</sup>, Qi Fan<sup>2</sup>, Gangshan Wu<sup>1</sup>, Xin Tao<sup>3</sup>, Limin Wang<sup>1†</sup>

<sup>1</sup>State Key Laboratory for Novel Software Technology, Nanjing University

<sup>2</sup> School of Intelligence Science and Technology, Nanjing University

<sup>3</sup> Kling Team, Kuaishou Technology

chienliang03@gmail.com lmwang@nju.edu.cn

## Abstract

*The quadratic complexity of the attention mechanism severely limits the context scalability of Video Diffusion Transformers (DiTs). We find that the highly sparse spatio-temporal attention patterns exhibited in Video DiTs can be naturally represented by the Monarch matrix. It is a class of structured matrices with flexible sparsity, enabling sub-quadratic attention via an alternating minimization algorithm. Accordingly, we propose VMonarch, a novel attention mechanism for Video DiTs that enables efficient computation over the dynamic sparse patterns with structured Monarch matrices. First, we adapt spatio-temporal Monarch factorization to explicitly capture the intra-frame and inter-frame correlations of the video data. Second, we introduce a recomputation strategy to mitigate artifacts arising from instabilities during alternating minimization of Monarch matrices. Third, we propose a novel online entropy algorithm fused into FlashAttention, enabling fast Monarch matrix updates for long sequences. Extensive experiments demonstrate that VMonarch achieves comparable or superior generation quality to full attention on VBench after minimal tuning. It overcomes the attention bottleneck in Video DiTs, reduces attention FLOPs by a factor of 17.5, and achieves a speedup of over 5× in attention computation for long videos, surpassing state-of-the-art sparse attention methods at 90% sparsity.*

## 1. Introduction

Long context modeling is a critical challenge in modern deep learning, particularly in Video Diffusion Transformers (DiTs) aiming to generate long-duration videos [25, 38, 47, 59, 62]. Video DiTs face significant computational bottlenecks due to the quadratic complexity of vanilla attention. According to Wan-2.1 [47], the attention mechanism accounts for up to 95% of the total computation at a sequence length of one million tokens.

\*Work is done during internship at Kling Team, Kuaishou Technology.

†Corresponding author.

To address the efficiency issue of attention mechanisms in modeling long sequences, various sub-quadratic attention mechanisms [4, 7, 12, 34, 48, 51, 55–57, 63, 68] have been proposed. They mitigate the  $\mathcal{O}(N^2)$  complexity of vanilla attention, where  $N$  represents the sequence length, and can be broadly categorized into two main types: Sparse Attention [56, 63] and Linear Attention [4, 57]. Sparse Attention mechanisms reduce computation by focusing on a subset of relevant tokens using predefined [5, 10, 45, 51] or dynamic blockwise sparse patterns [34, 50, 56, 68, 69]. The complexity of Sparse Attention is reduced to  $\mathcal{O}(\tau N^2)$ , where  $1 - \tau$  is the sparsity ratio. However, improperly defined patterns or too aggressive sparsity ratios can lead to significant performance degradation [50, 69], and the actual efficiency gain is often less than expected due to overhead from managing sparse structures [50] and irregular memory access [58], which poses more challenges for hardware-efficient implementation [12, 63]. Linear Attention mechanisms [7, 48, 55] approximate the attention computation using kernel methods, reducing the complexity to  $\mathcal{O}(N)$ . While they offer significant efficiency improvements, Linear Attention methods often suffer from a performance gap compared to standard attention due to their low-rank structure, which limits their expressive power [14, 66].

Sparse Attention and Linear Attention can be viewed as two matrix compression strategies that exploit sparsity or low-rank structures, respectively. Notably, the attention matrices in video DiTs are high-rank and sparse, exhibiting strong block-diagonal structures due to the inherent spatiotemporal locality in video data. This indicates that sparsity-based methods are more suitable for Video DiTs [47, 51]. Unlike prior sparse attention methods that use ineffective fixed patterns or unstructured dynamic patterns that are inefficient to compute densely, MonarchAttention [60] constructs the sparse attention maps using dynamically updated structured Monarch matrices [11]. Monarch matrices are parameterized as the product of hardware-friendly block-diagonal matrices interleaved with permutations, and can model a wide class of linear transforms, such

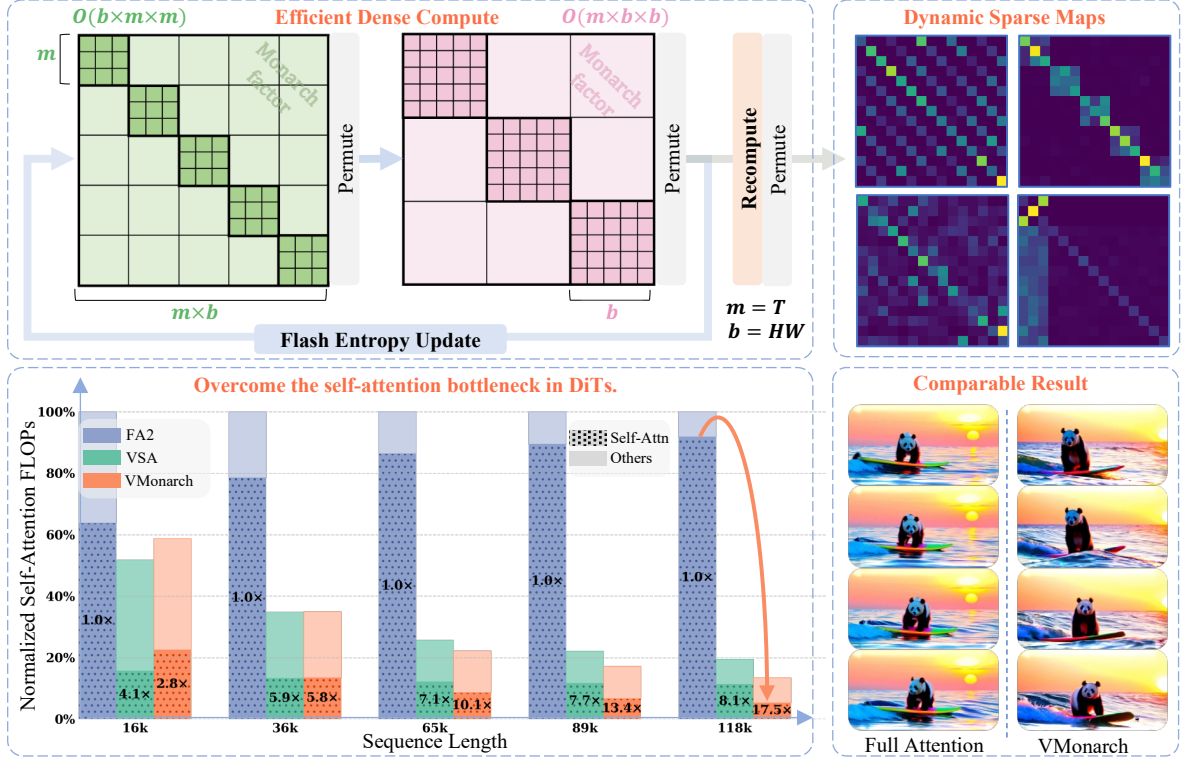


Figure 1. Video Monarch Attention (VMonarch) leverages dynamically updated spatial-temporal Monarch matrices [11] to model sparse attention patterns in video DiTs. When generating a 321-frame video at  $448 \times 832$  resolution (approximately 118K tokens), VMonarch speeds up self-attention computation by  $17.5 \times$  compared to full attention (FA2) [8] and by  $2 \times$  compared to highly sparse alternatives like Video Sparse Attention (VSA) at 90% sparsity. After minimal fine-tuning, VMonarch attains comparable video generation quality to FA2.

as Toeplitz matrices [17] and Butterfly matrices [9]. By alternately updating two dual Monarch matrices of size  $\sqrt{N}$  with an entropy-based regularization algorithm, Monarch Attention reduces the computational complexity to an optimal  $\mathcal{O}(N\sqrt{N})$ . This approach achieves a favorable balance between efficiency and expressiveness, making it particularly effective for modeling sparse structures.

However, directly applying Monarch Attention to Video DiTs presents several challenges: First, designing an effective block structure for Monarch matrices that captures both spatial and temporal dependencies in video is non-trivial, as the most efficient structure with monarch matrix sizes of  $\sqrt{N}$  can disrupt the inherent spatiotemporal structure of video data. Second, the inherent attention sink phenomenon in Video DiTs [51] causes the entropy-based regularization in MonarchAttention to be disproportionately focused on the first frame. This results in an excessively large softmax temperature, thereby degrading generation quality. Third, existing Monarch Attention implementations are not optimized for long sequences. Large monarch matrix sizes result in significant memory overhead during the alternating maximization updates, hindering the practical application to video modalities with very long sequences.

In this work, we propose Video Monarch Attention

(VMonarch), a novel and efficient framework that effectively integrates Monarch Attention into Video DiTs to address the aforementioned challenges. As shown in Fig. 1, our key contributions are summarized as follows:

- We are the first to explore representing the sparse attention maps in Video DiTs using Monarch matrices, for which we design a novel spatiotemporal block structure to capture dependencies in video data effectively, providing a new perspective on efficient attention mechanisms via structured matrix representations.
- To mitigate the quality degradation of the first frame due to excessive entropy regularization when updating Monarch matrices, we introduce a first-frame recomputation strategy that preserves the quality of the initial frame with modest computational overhead.
- We propose a novel online-entropy algorithm, analogous to the online softmax in FlashAttention [8], implemented in a customized GPU kernel to enable efficient Monarch matrix updating for long video sequences.
- Extensive experiments show that VideoMonarch attains comparable or superior generation quality to full attention on VBench after minimal fine-tuning, while achieving over  $17.5 \times$  attention FLOPs reduction with more than  $5 \times$  kernel speedup compared to FlashAttention-2 [8].

## 2. Related Work

**Diffusion Model Inference Acceleration.** Accelerating diffusion model inference has been an active area of research. Some works focus on reducing the computational cost of the denoising steps required during inference through techniques such as improved noise schedules [19, 32, 33, 35, 43, 44], knowledge distillation for fewer steps [41, 61], and reusing cached intermediate results [30, 36, 37]. Complementary to these methods, optimizing the attention mechanism with sparsification [5, 28, 50, 51, 56, 69] or linearization [16, 22, 54, 66] is an orthogonal approach that is crucial for accelerating diffusion model inference on long-sequence modalities, such as video, where attention computation becomes a significant bottleneck as the sequence length increases [47].

**Efficient Attention Mechanisms.** Sparse Attention mechanisms reduce the quadratic complexity of standard self-attention by limiting the number of key-value pairs to which each query attends. These mechanisms can be broadly categorized based on their sparsity patterns. Some methods employ fixed patterns to reduce attention computation, including local windowed attention [1], strided or dilated attention [1, 64],  $\Lambda$ -shape Pattern [53], Vertical-Slash Pattern [23], and so on. However, these fixed patterns may lack adaptability to varying input data. Other methods utilize dynamic patterns that adapt to the input data, such as dynamic block sparse attention [12, 26, 34, 42, 45, 50, 56, 63, 68, 69] and clustering-based attention mechanisms that regroup key-value pairs using k-means or locality-sensitive hashing (LSH) [6, 24, 31]. These dynamic methods often achieve better performance by tailoring the attention to the input, but they may incur additional computational overhead due to their unstructured dynamic patterns [58]. Another line of work focuses on Linear Attention mechanisms [2, 14, 20, 27, 29, 40, 54, 57, 57], which approximate the standard attention mechanism by reordering computations to achieve linear complexity with respect to the sequence length. Linear Attention demonstrates considerable inference efficiency (KV cache-free) [40, 57] under causal settings and offers superior computation savings in non-causal settings [13, 14, 18, 49] due to its linear complexity. SANA-Video [4] successfully applies blockwise linear attention to Video DiTs with a high-compression VAE. However, these methods are often limited by expressiveness due to their low-rank properties [14, 66], which need to be compensated for by hybrid architectures [2, 20, 27, 29], rank augmentation techniques [14], and state expansion [57]. Some works combine both sparse and linear attention mechanisms to model the high-rank and low-rank components of attention

matrices, respectively [3, 66]. These hybrid approaches enable sparse attention to leverage a higher sparsity ratio by using linear attention to capture the global context, indicating the importance of leveraging the inherent structure within attention matrices. There are also works exploring quantized attention mechanisms [65, 67], which reduce the precision of attention computation to lower bit-widths, thereby decreasing memory usage and computational load while maintaining performance. However, quantized methods are constrained by hardware precision formats and often suffer from accuracy degradation.

**Monarch Matrix.** Monarch matrices are a family of structured matrices that are hardware-efficient and expressive, as they are parameterized as the products of block-diagonal matrices interleaved with permutation operations. They can represent a wide class of transforms, including convolution, Hadamard transforms, Toeplitz matrices [17], Butterfly matrices [9] and AFDF matrices [39]. Previous works [11, 15] have shown the efficiency and effectiveness of Monarch matrices by applying them to neural network sparsification. Monarch matrices can be computed densely [15] by leveraging their block-diagonal structure, and they have a complexity from  $\mathcal{O}(N \log N)$  to  $\mathcal{O}(N^{3/2})$  depending on the number of Monarch factors [11], offering flexible sparsity. Moreover, MonarchAttention [60] uses Monarch matrices to approximate the attention map using an alternating minimization method, which demonstrates effectiveness in modeling a sparse attention map.

## 3. Method

### 3.1. Preliminaries

**Monarch Matrix** is a row-permuted block rank-one matrix [11]. Formally, given  $N = m \times b$  for integers  $m$  and  $b$ , we can define a Monarch matrix  $\mathbf{M} \in \mathbb{R}^{N \times N}$  by

$$\mathbf{M} = \mathbf{P}_{(b,N)} \mathbf{L} \mathbf{P}_{(b,N)}^\top \mathbf{R},$$

where  $\mathbf{L}$  and  $\mathbf{R}$  are two block-diagonal matrices called Monarch factors:  $\mathbf{L} = \text{diag}(\mathbf{L}_0, \dots, \mathbf{L}_{b-1})$  and  $\mathbf{R} = \text{diag}(\mathbf{R}_0, \dots, \mathbf{R}_{m-1})$ ;  $\mathbf{P}_{(b,N)}$  is a permutation matrix, whose  $(i+1)$ -th row is defined by  $e_{\sigma_{(b,N)}(i)}$  and  $\sigma_{(b,N)}(i) = i \bmod b + \lfloor i/b \rfloor \cdot b$ <sup>1</sup>. Write  $\mathbf{M}$  in block matrix form.  $M_{ijkl}$  is the  $(j, l)$  element in the  $(i, k)$  matrix. Denote the  $(j, k)$  element in  $\mathbf{L}_i$  as  $L_{ijk}$ . It can be derived that  $M_{ijkl} = L_{ijk} R_{kil}$ .

**Monarch Attention** [60] uses the Monarch matrix to approximate attention in the Transformer [46], which means finding a Monarch matrix  $\mathbf{M} \approx \text{softmax}(\mathbf{Q} \mathbf{K}^\top)$  and computing  $\mathbf{O} = \mathbf{M} \mathbf{V}$  to obtain the approximate result. To

<sup>1</sup>Applying  $\mathbf{P}_{(b,N)}$  to a length  $n$  vector means reshaping it into an  $m \times b$  matrix in row-major order, transposing it, and then flattening it back to a vector in row-major order.

avoid the computation of  $\sigma(\mathbf{Q}\mathbf{K}^\top)$ , MonarchAttention first rewrites softmax as an optimization problem.

$$\sigma(\mathbf{Q}\mathbf{K}^\top) = \underset{\mathbf{A} \in \Delta^{N \times N}}{\operatorname{argmax}} \langle \mathbf{A}, \mathbf{Q}\mathbf{K}^\top \rangle + H(\mathbf{A}), \quad (1)$$

where  $\Delta^{N \times N}$  denotes the set of row-stochastic matrices, and  $H(\mathbf{A}) = -\sum_{ij} \mathbf{A}_{ij} \log \mathbf{A}_{ij}$  is Shannon entropy. When  $\mathbf{A}$  is a Monarch matrix, we have

$$\begin{aligned} \langle \mathbf{M}, \mathbf{Q}\mathbf{K}^\top \rangle + H(\mathbf{M}) &= \langle \mathbf{PM}, \mathbf{PQK}^\top \rangle + H(\mathbf{PM}) \\ &= \langle \mathbf{PM}, \tilde{\mathbf{Q}}\mathbf{K}^\top \rangle + H(\mathbf{PM}) \\ &= \sum_{ik} \langle \mathbf{L}_{ik} \mathbf{R}_{ki}^\top, \tilde{\mathbf{Q}}_i \mathbf{K}_k^\top \rangle + H(\mathbf{L}_{ik} \mathbf{R}_{ki}^\top), \end{aligned} \quad (2)$$

where  $\mathbf{Q} = \{\mathbf{Q}_i\}_{i=1}^b$  and  $\mathbf{K} = \{\mathbf{K}_i\}_{i=1}^m$ . MonarchAttention uses alternating maximization to optimize the objective under the fact that when one component is fixed, the problem is concave. We can derive the closed-form solution.

$$\left\{ \begin{array}{l} \mathbf{R} = \operatorname{softmax}_l \left( \sum_v \alpha_{\mathbf{R},kiv} \mathbf{K}_{kiv} / c_{\mathbf{R},ki} \right) \\ \alpha_{\mathbf{R},kiv} = \sum_j \mathbf{L}_{ikj} \mathbf{Q}_{ijv}, \quad c_{\mathbf{R},ki} = \sum_j \mathbf{L}_{ikj}, \end{array} \right. \quad (3)$$

$$\left\{ \begin{array}{l} \mathbf{L} = \operatorname{softmax}_j \left( \sum_v \alpha_{\mathbf{L},ikv} \mathbf{Q}_{ijv} - c_{\mathbf{L},ik} \right) \\ \alpha_{\mathbf{L},ikv} = \sum_l \mathbf{R}_{kil} \mathbf{K}_{kiv}, \quad c_{\mathbf{L},ik} = \sum_l \mathbf{R}_{kil} \log \mathbf{R}_{kil}, \end{array} \right. \quad (4)$$

where  $\operatorname{softmax}_i$  means applying the softmax in dimension  $i$ , and  $\mathbf{Q}_{ijv}$  refers to the  $v$ -th element in the  $j$ -th column of  $\mathbf{Q}_i$ . After  $t$  iterations, the approximating result  $\mathbf{M}^{(t)}$  is obtained using  $\mathbf{L}^{(t)}, \mathbf{R}^{(t)}$ , and the output of attention can be calculated by  $\mathbf{O} = \mathbf{L}^{(t)} \mathbf{R}^{(t)} \mathbf{V}$ . The complexity of calculating  $\mathbf{R}$  and  $\mathbf{L}$  is  $\mathcal{O}(m(bmd))$  and  $\mathcal{O}(b(mbd))$ , respectively; therefore, the total complexity is  $\mathcal{O}(tN(m+b)d)$ . MonarchAttention can reduce the computational complexity from  $\mathcal{O}(N^2d)$  to  $\mathcal{O}(tN(m+b)d)$ , where  $t$  is a small constant.

**Implementation.** As shown in Fig. 2, the input matrices  $\mathbf{Q}, \mathbf{K}, \mathbf{V}$  are first reshaped from  $\mathbb{R}^{N \times d}$  to  $\mathbb{R}^{m \times b \times d}$ . The matrices  $\mathbf{Q}$  and  $\mathbf{K}$  are then used to calculate the monarch factors  $\mathbf{L}$  and  $\mathbf{R}$  by iteratively applying the closed-form solution. To minimize data movement and memory usage on GPUs, MonarchAttention combines (Eq. (3), Eq. (6)) into a kernel and (Eq. (4), Eq. (5)) into another. Specifically, it stores  $\alpha_{\mathbf{L}}, c_{\mathbf{L}}, \alpha_{\mathbf{R}}, c_{\mathbf{R}}$  in the loop and only writes  $\mathbf{L}$  and  $\mathbf{R}$  in the last iteration. After the iteration, the output of MonarchAttention can be calculated by the multiplication of  $\mathbf{L}, \mathbf{R}$ , and  $\mathbf{V}$ , interleaved with permutation. The detailed Python-like code can be found in Sec. A.

### 3.2. Video Monarch Attention

Video DiTs often exhibit a sparse, block-diagonal attention structure. Tokens within the same frame or adjacent pixels tend to have stronger interactions; this inherent structure aligns well with the sparse block-diagonal properties of

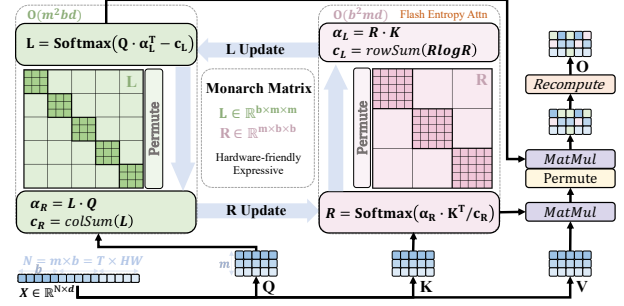


Figure 2. Overview of our Video Monarch Attention. (a) We represent the  $N \times N$  full attention matrix via two alternatingly optimized smaller Monarch factors  $\mathbf{L}$  and  $\mathbf{R}$  with spatial-temporal structure factorization. (b) We introduce a Recomputation Strategy to address quality degradation caused by excessively large temperature term  $c_{\mathbf{R}}$  for the first frame. (c) We propose an Online-Entropy algorithm integrated with FlashAttention to accelerate the iterative computation of Monarch matrices further.

Monarch matrices. To leverage this prior, we propose Video Monarch Attention, which adapts the Monarch matrix factorization with a spatio-temporal structure tailored for video DiTs. For a video sequence consisting of  $T$  frames, with each frame containing  $H \times W$  spatial tokens, thus resulting in a total of  $N = THW$  tokens, we set the Monarch matrix parameters  $m = T$  and  $b = H \times W$ . This aligns the block structure of the Monarch matrix with the spatio-temporal layout of video tokens.

Formally, given the queries  $\mathbf{Q} \in \mathbb{R}^{N \times d}$ , keys  $\mathbf{K} \in \mathbb{R}^{N \times d}$ , and values  $\mathbf{V} \in \mathbb{R}^{N \times d}$ , we compute the Video Monarch Attention output as:

$$\mathbf{O} = \operatorname{MonarchAttention}(\mathbf{Q}, \mathbf{K}, \mathbf{V}; m, b, t), \quad (7)$$

where the MonarchAttention function utilizes the Monarch matrices defined by  $m = T$  and  $b = HW$  and performs  $t = 2$  iterations of alternating optimization. During the iterative optimization of the Monarch factors  $\mathbf{L}$  and  $\mathbf{R}$ , we maintain the spatio-temporal structure by ensuring that  $\mathbf{L} \in \mathbb{R}^{m^2 \times b}$  captures temporal dependencies across frames, while  $\mathbf{R} \in \mathbb{R}^{b^2 \times m}$  captures spatial dependencies within each frame. This allows Video Monarch Attention to efficiently approximate the full attention map by factorizing it into dedicated spatial and temporal components while maintaining computational efficiency.

**Complexity Analysis.** As we set  $m = T$  and  $b = HW$  to align with the spatio-temporal structure of video data, and utilize  $t$  iterations for the alternating optimization, the computational complexity of Video Monarch Attention becomes  $\mathcal{O}(tN(T + HW)d)$ . Given  $N = THW$  and  $T \ll HW$ , this yields a theoretical speedup of  $\frac{THW}{t(T+HW)} \approx \frac{T}{t}$  over the standard  $\mathcal{O}(N^2d)$  attention.

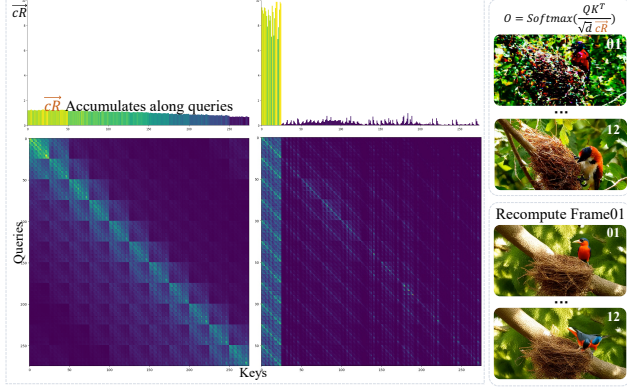


Figure 3. Illustration of the attention sink phenomenon in video models. The first frame tends to accumulate excessive attention from subsequent frames, leading to a loss of fine-grained details when using Monarch Attention. Our First-Frame Recomputation Strategy effectively restores these details by recalculating the attention for the first frame using full attention.

### 3.3. First-Frame Recomputation Strategy

In video DiTs, there exists a well-known attention sink phenomenon in the first frame [28, 51, 52], where the initial frame serves as a crucial contextual anchor for the entire sequence and tends to attract disproportionate attention from subsequent frames. We observe that this attention sink phenomenon negatively impacts the performance of Video Monarch Attention, as shown in Fig. 3. As the first frame tokens receive excessive cumulative attention score during the iterative optimization of Monarch Attention, the temperature adjustment term  $c_R$  for these tokens becomes significantly large. This leads to a smoother attention distribution, causing degradation in the generation quality of the first frame.

To mitigate this issue, we introduce a simple yet effective First-Frame Recomputation Strategy. We explicitly recompute the attention outputs for the first frame using full attention, as shown in Fig. 2. Specifically, we take the queries  $Q_0$  corresponding to the first frame, keys  $K$ , and values  $V$ , and compute the attention output as:

$$O_0 = \text{softmax} \left( \frac{Q_0 K^\top}{\sqrt{d}} \right) V. \quad (8)$$

This recomputation step introduces a modest computational overhead. The cost is  $\mathcal{O}(bNd)$ , specifically  $\frac{b}{t(m+b)}$  of the total cost of Video Monarch Attention. This ensures that we can restore the fidelity of the first frame without compromising the overall efficiency of our method.

### 3.4. Online Entropy Based FlashAttention

Upon profiling Video Monarch Attention, we identify the primary computational bottleneck in the update step for the  $R$  matrix and its entropy term  $c_L$  ( Eq. (3), Eq. (6)). The

---

#### Algorithm 1 Flash-Entropy-Attention

---

**Require:**  $Q, K, V \in \mathbb{R}^{N \times d}$ , Block sizes  $B_c, B_r$ .  
**Ensure:**  $O \in \mathbb{R}^{N \times d}, L \in \mathbb{R}^N, H \in \mathbb{R}^N$  (Entropy).

- 1:  $T_r \leftarrow \lceil N/B_r \rceil, T_c \leftarrow \lceil N/B_c \rceil$ .
- 2: **for**  $i = 1 \rightarrow T_r$  **do**
- 3:     Load  $Q_i$  to SRAM.
- 4:     **for**  $j = 1 \rightarrow T_c$  **do**
- 5:         Load  $K_j, V_j$  to SRAM.
- 6:          $S_{ij} \leftarrow Q_i K_j^\top$ .
- 7:          $m_i^{(j)} \leftarrow \max(m_i^{(j-1)}, \text{rowmax}(S_{ij}))$ .
- 8:          $P_{ij} \leftarrow \exp(S_{ij} - m_i^{(j)})$ .
- 9:          $\alpha \leftarrow \exp(m_i^{(j-1)} - m_i^{(j)})$ .
- 10:          $O_i^{(j)} \leftarrow \text{diag}(\alpha) O_i^{(j-1)} + P_{ij} V_j$ .
- 11:          $\ell_i^{(j)} \leftarrow \alpha \odot \ell_i^{(j-1)} + \text{rowsum}(P_{ij})$ .
- 12:          $h_i^{(j)} \leftarrow \alpha \odot h_i^{(j-1)} + \alpha \log(\alpha) \odot \ell_i^{(j-1)} + \text{rowsum}(P_{ij} \log(P_{ij}))$ .
- 13:     **end for**
- 14:      $O_i \leftarrow \text{diag}(\ell_i^{(T_c)})^{-1} O_i^{(T_c)}$ .
- 15:      $L_i \leftarrow m_i^{(T_c)} + \log(\ell_i^{(T_c)})$ .
- 16:      $H_i \leftarrow \log(\ell_i^{(T_c)}) - h_i^{(T_c)} / \ell_i^{(T_c)}$ .
- 17:     Write  $O_i, L_i, H_i$  to HBM.
- 18: **end for**

---

complexity of this step is  $\mathcal{O}(mb^2d)$ , where  $m$  corresponds to the number of frames  $T$ , and  $b$  to the spatial tokens per frame ( $H \times W$ ). In typical video generation scenarios, the spatial dimension is significantly larger than the temporal one ( $b \gg m$ ), causing the  $b^2$  term to dominate the computation and rendering a naive implementation inefficient. To address this, we propose an online-entropy based FlashAttention algorithm that computes the softmax attention output and the entropy in a single pass, significantly reducing data movement between HBM and on-chip SRAM and improving computational efficiency in the Monarch factor  $R$  updating. The forward and backward passes are provided in Algorithm 1 and Algorithm 2 (see Appendix), respectively.

## 4. Experiments

### 4.1. Implementation Setup

**Base Model and Datasets.** We conduct experiments on three base models: Wan2.1-1.3B, Wan2.1-14B, and Wan2.2-5B [47]. To adapt the attention mechanism, we utilize the Wan14B-Syn-600k dataset [69] for the 1.3B model, and the Wan2.2-Syn-32k dataset [69] for the larger 14B and 5B models. We compare our VMonarch with current state-of-the-art sparse attention-based methods in Video DiTs, including VSA [69] and VMoBA [50], and choose FlashAttention-2 [8] as our full attention backend.

**Metrics.** Following prior works [50, 59], we use VBench [21] prompts after optimization for the evaluation of all models. We adopt five assessment aspects from VBench to evaluate the video generation quality. Specifi-

Table 1. Quality and efficiency comparison of our and other methods, including Full Attention [8], VSA [69], and VMoBA [50]. We verify the generalizability of our method across different architectures, parameter scales, and varying resolutions under the same tuning setting. We report Vbench [21] metrics to evaluate quality, including Aesthetic Quality (AQ), Background Consistency (BC), Dynamic Degree (DD), Imaging Quality (IQ), and Subject Consistency (SC). We also report the efficiency metrics, including attention sparsity, TFLOPs, and inference time.  $\circlearrowleft$  denotes Training-Free setting.  $*$  denotes extrapolation on longer sequences using the Wan2.1-1.3B [47] model tuned at  $61 \times 448 \times 832$  resolution. We highlight the results of VMonarch if it is the **best** or second best among efficient attention methods.

Model	Resolution	Kernel	Quality					Efficiency		
			AQ $\uparrow$	BC $\uparrow$	DD $\uparrow$	IQ $\uparrow$	SC $\uparrow$	Sparsity $\uparrow$	TFLOPs $\downarrow$	Time (s) $\downarrow$
Wan2.1 1.3B	61x448x832	FullAttn $\circlearrowleft$	65.44%	95.08%	69.44%	64.86%	91.77%	-	159.7	63.4
		VMoBA $\circlearrowleft$	42.00%	90.64%	88.89%	53.78%	82.00%	90.0%	75.8	71.7
		VSA $\circlearrowleft$	42.86%	94.96%	63.89%	55.04%	89.17%	90.0%	69.5	49.9
		VMonarch $\circlearrowleft$	<b>63.65%</b>	<b>94.93%</b>	54.17%	<b>64.46%</b>	<b>92.43%</b>	87.5%	75.4	<b>47.7</b>
	61x720x1280	FullAttn	66.07%	95.75%	68.06%	64.57%	94.15%	-	159.7	63.4
		VMoBA	65.58%	96.22%	62.50%	66.70%	93.00%	90.0%	75.8	71.7
		VSA	64.46%	95.09%	61.11%	63.87%	92.99%	90.0%	69.5	49.9
		VMonarch	<b>65.58%</b>	<b>95.84%</b>	<b>62.50%</b>	<b>64.49%</b>	<b>93.23%</b>	87.5%	75.4	<b>47.7</b>
Wan2.1 1.3B*	61x720x1280	FullAttn	65.49%	96.03%	76.39%	65.15%	93.64%	-	758.9	246.8
		VSA	65.07%	95.86%	63.89%	65.69%	92.07%	90.0%	208.6	125.8
	141x448x832	VMonarch	<b>64.39%</b>	<b>96.13%</b>	<b>69.44%</b>	<b>65.84%</b>	<b>93.82%</b>	87.5%	243.3	<u>136.8</u>
		FullAttn	64.27%	92.73%	63.89%	61.28%	92.63%	-	640.5	214.2
		VSA	63.04%	92.21%	66.67%	59.80%	89.71%	90.0%	184.2	112.6
	93x704x1280	VMonarch	<b>60.45%</b>	<b>92.25%</b>	<b>69.44%</b>	<b>59.92%</b>	<b>88.86%</b>	94.4%	170.2	<b>102.7</b>
		FullAttn $\circlearrowleft$	67.42%	96.02%	66.67%	66.73%	93.52%	-	7903.8	2222.2
		FullAttn	67.49%	97.04%	61.11%	68.53%	95.23%	-	7903.8	2222.2
		VSA	66.40%	96.93%	59.72%	65.91%	94.05%	90.0%	2642.7	970.9
	Wan2.2 5B	VMonarch	<b>65.91%</b>	<b>97.32%</b>	<b>58.33%</b>	<b>66.61%</b>	<b>95.68%</b>	92.0%	2670.5	<b>969.2</b>
		FullAttn $\circlearrowleft$	64.66%	96.10%	72.22%	65.24%	93.58%	-	352.4	123.7
		FullAttn	64.99%	96.67%	62.50%	65.44%	94.56%	-	352.4	123.7
		VSA	64.82%	96.30%	61.11%	65.26%	93.29%	90.0%	204.4	103.0
	93x704x1280	VMonarch	<b>65.04%</b>	<b>96.68%</b>	<b>59.72%</b>	<b>66.69%</b>	<b>94.20%</b>	92.0%	205.5	<b>92.0</b>

ally, we choose Aesthetic Quality (AQ), Background Consistency (BC), Dynamic Degree (DD), Imaging Quality (IQ), and Subject Consistency (SC) as our evaluation metrics. Furthermore, we use Peak Signal to Noise Ratio (PSNR) to evaluate the similarity between efficient attention and full attention generated videos.

**Definition of Sparsity.** VSA uses a top-k strategy with a fixed 90% sparsity ratio, and VMoBA uses a top-p strategy with 0.25 threshold; we approximate it to 90% sparsity for reference. We estimate the sparsity of VMonarch as  $1 - t \cdot \frac{T+HW}{THW} \approx 1 - \frac{t}{T}$ <sup>2</sup>, where  $t$  is the Monarch iteration number and  $THW$  is the latent size (with  $HW \gg T$ ).

**Implementation details.** We fine-tune all models using the AdamW optimizer with a learning rate of  $1 \times 10^{-6}$  and a batch size of 8. Specifically, for Wan2.1-1.3B, we fine-tune the DiT backbone for 1500 steps at a resolution of  $61 \times 448 \times 832$ . For Wan2.1-14B and Wan2.2-5B, we fine-tune them for 800 steps at a resolution of

<sup>2</sup>Two Monarch factors  $L \in \mathbb{R}^{m \times b \times b}$  and  $R \in \mathbb{R}^{b \times m \times m}$ , letting  $n = m \times b$ , result in  $1 - \frac{m+b}{n}$  sparsity to  $n \times n$  matrices.

$93 \times 704 \times 1280$ , utilizing sequence parallelism of size 8. For VMonarch, we set the block size to the number of tokens in one frame, *i.e.*  $HW$ , and clamp the  $c_R$  value to 0.1 for numerical stability and use two Monarch iterations by default. For VSA and VMoBA, we follow their official default configurations. We did not employ common training-free tricks such as hybridizing with Full Attention in layers, heads, or early denoising steps, which could potentially improve performance. During inference, we apply the same attention kernel across 50 denoising timesteps, without using full attention for the initial steps, as in prior works [50, 51]. Except for the attention kernel, all other inference settings are the same. This ensures a fair comparison of end-to-end performance across different attention mechanisms. For sequence length extension experiments, we evaluate the above fine-tuned models in spatial dimensions extension ( $61 \times 720 \times 1280$ ) and temporal dimensions extension ( $141 \times 448 \times 832$ ). VMoBA is omitted due to chunk-divisibility requirements. See Sec. D for details.

Table 2. Ablation studies on training-free setting. In 'VM-Tn-Fk', T represents the number of iterations, and F denotes the size of the Monarch factor  $b$  corresponding to the number of frames. The  $\dagger$  indicates the model variant without first frame computation.

Model	Similarity		Vbench Score (%)				
	PSNR $\uparrow$	SSIM $\uparrow$	AQ	BC	DD	IQ	SC
Softmax	-	-	65.44	95.08	69.44	64.86	91.77
VM-T1-F1	11.18	0.35	54.36	89.75	16.67	54.93	93.17
VM-T2-F1 $\dagger$	11.65	0.40	63.39	92.25	29.17	67.76	88.46
VM-T2-F1	12.59	0.43	63.65	94.93	54.17	64.46	92.43
VM-T3-F1	12.21	0.41	63.89	95.01	50.00	65.12	93.55
VM-T1-F2	11.21	0.35	55.27	89.80	20.83	56.44	93.09

## 4.2. Method Effectiveness

**Quantitative Results.** We present the quantitative results of our Video Monarch Attention compared to other baseline methods in Tab. 1. In the training-free setting, both our Monarch Attention and other sparse attention methods exhibit a performance drop compared to the original full attention. This is expected, as the base model has not been adapted to the inductive biases of efficient attention kernels. However, we observe that Monarch Attention significantly outperforms other sparse attention methods under high sparsity ratios (90%), which we attribute to its preservation of the global spatio-temporal structure inherent in video data. We also note a significant decrease in the Dynamic Degree for Monarch Attention in the training-free setting. We hypothesize that this is due to the approximation error from the alternating minimization optimization of the Monarch matrix. Nevertheless, VMonarch’s performance on Dynamic Degree is fully restored after minimal fine-tuning for 1500 steps, even surpassing the original full attention, while also outperforming other sparse attention-based models in Subject Consistency and Aesthetic Quality. We evaluate the zero-shot generalization of the fine-tuned model with spatial and temporal sequence length extension. VMonarch demonstrates remarkable generalization capabilities. For temporal extension to  $141 \times 448 \times 832$ , it achieves results comparable to the original model while being superior to VSA. In the spatial extension setting of  $61 \times 720 \times 1280$ , our method again performs exceptionally well, outperforming both VSA and full attention on several key metrics, including Background Consistency, Dynamic Degree, Imaging Quality, and Subject Consistency, which demonstrates the powerful expressive capability of VMonarch. VMonarch also maintains comparable or even superior performance to other methods across larger parameter scales and extended sequence lengths, verifying its strong generalizability.

**Qualitative Results.** As shown in Fig. 4, we present qualitative samples generated by Wan2.1-1.3B fine-tuned under identical settings. The results demonstrate that

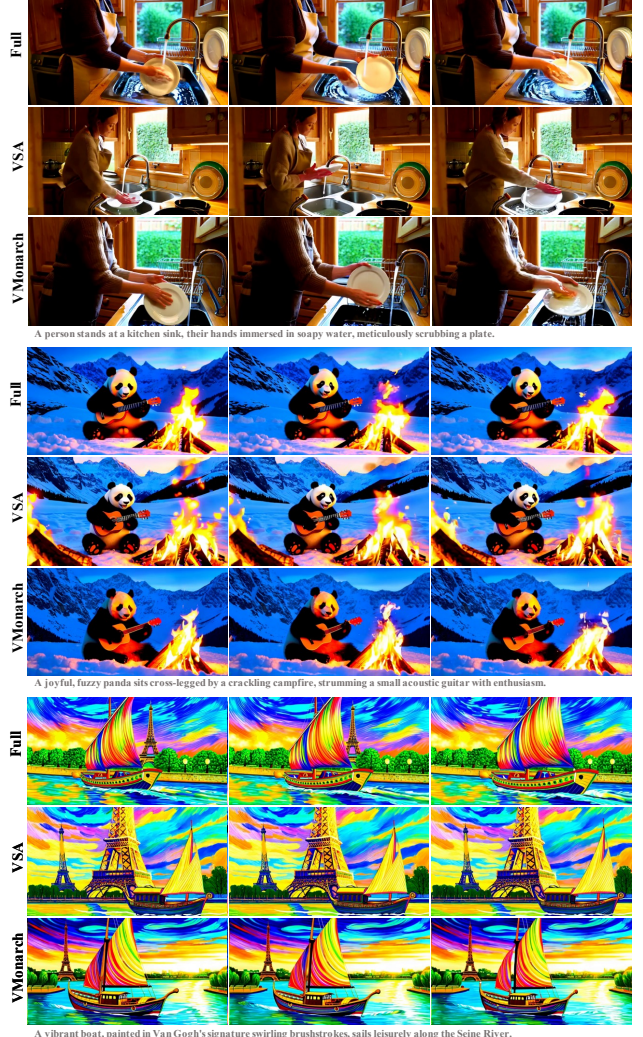


Figure 4. Qualitative samples of our models. We compare the generation quality of the tuned models between full attention [8], Video Sparse Attention (VSA) [69], and our VMonarch Attention.

VMonarch generates videos with a quality comparable to that of full attention. In contrast, VSA occasionally produces incoherent content. This suggests that VMonarch better captures the spatio-temporal priors inherent in video generation, leading to more robust and consistent results.

## 4.3. Method Efficiency

As shown in Tab. 1, we evaluate the efficiency of different attention mechanisms in terms of FLOPs and end-to-end inference time. The FLOPs of VMoBA is estimated at an equivalent 90% sparsity for comparison. Our VMonarch utilizes an estimated sparsity  $(1 - t \cdot \frac{T+HW}{THW})$ , where  $t$  is the iteration number (set to 2),  $(T, H, W)$  is the latent token shape. In the  $61 \times 448 \times 832$  setting, VMonarch reduces TFLOPs by 53% and inference time by 25% compared to full attention, even surpassing VSA which has

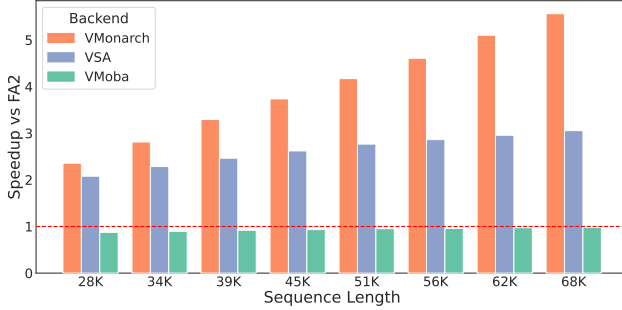


Figure 5. The kernel speedup ratio over Flash Attention 2 (FA2) [8] under varying sequence lengths. Our VMonarch demonstrates superior efficiency, achieving over  $2\times$  speedup at 28k tokens and over  $5\times$  speedup at 62k tokens compared to FA2, surpassing other sparse attention methods at 90% sparsity.

lower TFLOPs, exhibiting superior practical efficiency from VMonarch’s structured computation. This efficiency advantage becomes more pronounced in long-sequence scenarios. For temporal extension to  $141 \times 448 \times 832$ , VMonarch achieves a  $2.1\times$  speedup over full attention and is also 9% faster than VSA. As shown in Fig. 5, we also benchmark the kernel-level speed, gradually increasing the token number from 30k to 60k by varying the number of latent temporal dimensions from 20 to 48 under (28, 52) spatial size. The Monarch matrix size is set with spatial-temporal structure; VSA and VMoBA’s block number is set to match the sparsity ratio of 90%. Our VMonarch demonstrates significant efficiency gains, achieving over  $2\times$  speedup compared to FA2 at 34k tokens and over  $5\times$  speedup at 62k tokens. Furthermore, VMonarch achieves an  $8\times$  speedup over the naive implementation when optimized with Online-Entropy Flash Attention, with details in Sec. F.

#### 4.4. Ablation Studies

**Number of iterations.** We investigate the impact of the number of iterations on Monarch Attention’s performance. In the training-free setting, as shown in Tab. 2, increasing the iterations from 1 to 3 gradually improves most VBench metrics, with the Dynamic Degree peaking at two iterations. As shown in Tab. 3, after fine-tuning, more iterations lead to a lower validation loss, indicating a stronger fitting capability but at the cost of increased computation. Extending the number of iterations up to 7 yields no significant gains while reducing efficiency. Notably, the 2-iteration setting strikes an optimal balance between effectiveness and efficiency, outperforming the 3-iteration setting on Dynamic Degree with less computational overhead. Therefore, we adopt two Monarch iterations as our default.

**Monarch matrix size.** We set the Monarch matrix size  $b$  to the number of tokens in a single frame by default, *i.e.*,  $b = HW$ , to align with the natural structure of video data. We compare this with a larger block size spanning

Table 3. Ablation studies on fine-tuned Video Monarch Attention models under different configurations. In ‘VM-Tn-Fk’, T represents iterations numbers, and F denotes the frame number corresponding to the Monarch Matrix  $b$ .  $\dagger$  omits the recompute strategy for the first frame.  $\ddagger$  means leveraging attention sink by averaging.

Model	Vbench Score (%)					Val Loss
	AQ	BC	DD	IQ	SC	
Softmax	65.72	94.85	75.00	64.46	92.59	1.09
VM-T1-F1	66.53	95.82	59.72	65.28	92.69	1.27
VM-T2-F1	64.84	95.28	68.06	63.83	93.29	1.25
VM-T3-F1	66.22	96.12	56.94	65.72	94.06	1.24
VM-T5-F1	65.63	96.16	45.83	67.91	94.94	1.57
VM-T7-F1	64.39	96.71	36.11	65.51	94.61	1.55
VM-T1-F2	66.90	96.61	55.56	65.05	94.44	1.37
VM-T2-F1 $\dagger$	63.22	92.19	69.44	63.63	87.36	1.27
VM-T2-F1 $\ddagger$	63.85	94.94	45.83	67.40	93.83	1.78

two frames ( $b = 2HW$ ). As shown in Tab. 2 and Tab. 3, under the training-free setting, while the larger block size ( $b = 2F$ ) shows a slight improvement on metrics, it introduces visual temporal inconsistency artifacts, with abrupt changes occurring every two frames. This is due to a structural mismatch between the matrix size and the video’s spatial-temporal structure. This partitioning-induced artifact is not resolved by fine-tuning. The model with  $b = 2F$  results in a higher validation loss, reduced Dynamic Degree and Imaging Quality. This underscores the importance of aligning the Monarch block structure with the intrinsic spatial-temporal structure of video data.

**First-frame recomputation.** We analyze the effectiveness of our proposed first-frame recomputation strategy in mitigating oversmoothing in the first frame. Under training-free settings, as shown in Tab. 2, omitting the first-frame computation results in a significant drop in PSNR and SSIM, as well as almost all VBench metrics, indicating a substantial deviation from the full attention output.

To further isolate the impact on the initial frame, we additionally calculate the PSNR and SSIM on the first frame only. With our recomputation strategy, the first frame achieves a PSNR of 12.43 and an SSIM of 0.42. In contrast, without recomputation, these scores drop to 10.42 and 0.34, respectively, which underscores the necessity of the recomputation strategy for preserving first-frame quality.

As shown in Tab. 3, we evaluate our first-frame recomputation strategy by comparing it against two alternatives under the fine-tuning setting: one that omits the recomputation ( $\dagger$ ), and another that uses an attention sink mechanism ( $\ddagger$ ). The latter approach ( $\ddagger$ ) computes the output by averaging the standard Monarch Attention with full attention to the first frame, defined as  $O = (\text{Softmax}(Q, K_{F1}, V_{F1}) + \text{MonarchAttention}(Q, K, V))/2$ , where  $K_{F1}$  and  $V_{F1}$  are the key and value from the first frame. Compared to both

alternatives, our recomputation strategy demonstrates superior performance. The attention sink approach ( $\ddagger$ ) exhibited convergence issues during training, leading to a higher validation loss and degraded performance in Dynamic Degree and Subject Consistency. Our default strategy achieves a lower validation loss and higher scores across both image quality (Aesthetic Quality, Imaging Quality) and stability metrics (Background Consistency, Subject Consistency) compared to the variant without recomputation ( $\dagger$ ).

## 5. Conclusion

We overcome the quadratic complexity bottleneck in DiT-based video generation by introducing VMonarch, a sub-quadratic attention mechanism that leverages an expressive class of Monarch matrices with spatial-temporal structure. Furthermore, we introduce a first-frame recomputation strategy to mitigate initial frame artifacts caused by the over-smoothing issue during the iterative minimization of Monarch matrices. We also develop a custom GPU kernel that merges FlashAttention with online entropy computation, enabling VMonarch to process video sequences efficiently with fast updates of Monarch matrices. Extensive experiments demonstrate that VMonarch achieves a superior trade-off between quality and efficiency, maintaining generation quality comparable or superior to full attention on VBench while delivering more than  $5\times$  attention kernel speedup and over a  $17\times$  reduction in attention FLOPs for long video sequences.

## References

- [1] Iz Beltagy, Matthew E Peters, and Arman Cohan. Longformer: The long-document transformer. *arXiv preprint arXiv:2004.05150*, 2020. [3](#)
- [2] Aaron Blakeman, Aarti Basant, Abhinav Khattar, Adithya Renduchintala, Akhiad Bercovich, Aleksander Ficek, Alexis Bjorlin, Ali Taghibakhshi, Amala Sanjay Deshmukh, Ameya Sunil Mahabaleshwarkar, et al. Nemotron-h: A family of accurate and efficient hybrid mamba-transformer models. *arXiv preprint arXiv:2504.03624*, 2025. [3](#)
- [3] Beidi Chen, Tri Dao, Eric Winsor, Zhao Song, Atri Rudra, and Christopher Ré. Scatterbrain: Unifying sparse and low-rank attention. *Advances in Neural Information Processing Systems*, 34:17413–17426, 2021. [3](#)
- [4] Junsong Chen, Yuyang Zhao, Jincheng Yu, Ruihang Chu, Junyu Chen, Shuai Yang, Xianbang Wang, Yicheng Pan, Daquan Zhou, Huan Ling, et al. Sana-video: Efficient video generation with block linear diffusion transformer. *arXiv preprint arXiv:2509.24695*, 2025. [1, 3](#)
- [5] Pengtao Chen, Xianfang Zeng, Maosen Zhao, Peng Ye, Mingzhu Shen, Wei Cheng, Gang Yu, and Tao Chen. Sparse-vdit: Unleashing the power of sparse attention to accelerate video diffusion transformers. *arXiv preprint arXiv:2506.03065*, 2025. [1, 3](#)
- [6] Zhuoming Chen, Ranajoy Sadhukhan, Zihao Ye, Yang Zhou, Jianyu Zhang, Niklas Nolte, Yuandong Tian, Matthijs Douze, Leon Bottou, Zhihao Jia, et al. Magicpig: Lsh sampling for efficient llm generation, 2024. *URL https://arxiv.org/abs/2410.16179*. [3](#)
- [7] Krzysztof Choromanski, Valerii Likhoshesterov, David Dohan, Xingyou Song, Andreea Gane, Tamas Sarlos, Peter Hawkins, Jared Davis, Afroz Mohiuddin, Lukasz Kaiser, et al. Rethinking attention with performers. *arXiv preprint arXiv:2009.14794*, 2020. [1](#)
- [8] Tri Dao. Flashattention-2: Faster attention with better parallelism and work partitioning. *arXiv preprint arXiv:2307.08691*, 2023. [2, 5, 6, 7, 8, 3, 4](#)
- [9] Tri Dao, Nimit S Sohoni, Albert Gu, Matthew Eichhorn, Amit Blonder, Megan Leszczynski, Atri Rudra, and Christopher Ré. Kaleidoscope: An efficient, learnable representation for all structured linear maps. *arXiv preprint arXiv:2012.14966*, 2020. [2, 3](#)
- [10] Tri Dao, Beidi Chen, Kaizhao Liang, Jiaming Yang, Zhao Song, Atri Rudra, and Christopher Re. Pixelated butterfly: Simple and efficient sparse training for neural network models. *arXiv preprint arXiv:2112.00029*, 2021. [1](#)
- [11] Tri Dao, Beidi Chen, Nimit S Sohoni, Arjun Desai, Michael Poli, Jessica Grogan, Alexander Liu, Aniruddh Rao, Atri Rudra, and Christopher Ré. Monarch: Expressive structured matrices for efficient and accurate training. In *International Conference on Machine Learning*, pages 4690–4721. PMLR, 2022. [1, 2, 3, 5](#)
- [12] Juechu Dong, Boyuan Feng, Driss Guessous, Yanbo Liang, and Horace He. Flex attention: A programming model for generating optimized attention kernels. *arXiv preprint arXiv:2412.05496*, 2024. [1, 3](#)
- [13] Qihang Fan, Huaibo Huang, Yuang Ai, and Ran He. Rectifying magnitude neglect in linear attention. In *Proceedings of the IEEE/CVF International Conference on Computer Vision*, pages 21505–21514, 2025. [3](#)
- [14] Qihang Fan, Huaibo Huang, and Ran He. Breaking the low-rank dilemma of linear attention. In *Proceedings of the Computer Vision and Pattern Recognition Conference*, pages 25271–25280, 2025. [1, 3](#)
- [15] Dan Fu, Simran Arora, Jessica Grogan, Isys Johnson, Evan Sabri Eyuboglu, Armin Thomas, Benjamin Spector, Michael Poli, Atri Rudra, and Christopher Ré. Monarch mixer: A simple sub-quadratic gemm-based architecture. *Advances in Neural Information Processing Systems*, 36:77546–77603, 2023. [3](#)
- [16] Mohsen Ghafoorian, Denis Korzhenkov, and Amirhossein Habibian. Attention surgery: An efficient recipe to linearize your video diffusion transformer. *arXiv preprint arXiv:2509.24899*, 2025. [3](#)
- [17] Robert M Gray et al. Toeplitz and circulant matrices: A review. *Foundations and Trends® in Communications and Information Theory*, 2(3):155–239, 2006. [2, 3](#)
- [18] Dongchen Han, Yifan Pu, Zhuofan Xia, Yizeng Han, Xuran Pan, Xiu Li, Jiwen Lu, Shiji Song, and Gao Huang. Bridging the divide: Reconsidering softmax and linear attention. *Advances in Neural Information Processing Systems*, 37:79221–79245, 2024. [3](#)

[19] Jonathan Ho, Ajay Jain, and Pieter Abbeel. Denoising diffusion probabilistic models. *Advances in neural information processing systems*, 33:6840–6851, 2020. 3

[20] Jiancheng Huang, Gengwei Zhang, Zequn Jie, Siyu Jiao, Yinlong Qian, Ling Chen, Yunchao Wei, and Lin Ma. M4v: Multi-modal mamba for text-to-video generation. *arXiv preprint arXiv:2506.10915*, 2025. 3

[21] Ziqi Huang, Yinan He, Jiashuo Yu, Fan Zhang, Chenyang Si, Yuming Jiang, Yuanhan Zhang, Tianxing Wu, Qingyang Jin, Nattapol Chanpaisit, et al. Vbench: Comprehensive benchmark suite for video generative models. In *Proceedings of the IEEE/CVF Conference on Computer Vision and Pattern Recognition*, pages 21807–21818, 2024. 5, 6, 2

[22] Mude Hui, Rui-Jie Zhu, Songlin Yang, Yu Zhang, Zirui Wang, Yuyin Zhou, Jason Eshraghian, and Cihang Xie. Arflow: Autogressive flow with hybrid linear attention. *arXiv preprint arXiv:2501.16085*, 2025. 3

[23] Huiqiang Jiang, Yucheng Li, Chengruidong Zhang, Qianhui Wu, Xufang Luo, Surin Ahn, Zhenhua Han, Amir H Abdi, Dongsheng Li, Chin-Yew Lin, et al. Minference 1.0: Accelerating pre-filling for long-context llms via dynamic sparse attention. *Advances in Neural Information Processing Systems*, 37:52481–52515, 2024. 3

[24] Nikita Kitaev, Łukasz Kaiser, and Anselm Levskaya. Reformer: The efficient transformer. *arXiv preprint arXiv:2001.04451*, 2020. 3

[25] Weijie Kong, Qi Tian, Zijian Zhang, Rox Min, Zuozhuo Dai, Jin Zhou, Jiangfeng Xiong, Xin Li, Bo Wu, Jianwei Zhang, et al. Hunyuandvideo: A systematic framework for large video generative models. *arXiv preprint arXiv:2412.03603*, 2024. 1

[26] Xunhao Lai, Jianqiao Lu, Yao Luo, Yiyuan Ma, and Xun Zhou. Flexprefill: A context-aware sparse attention mechanism for efficient long-sequence inference. *arXiv preprint arXiv:2502.20766*, 2025. 3

[27] Aonian Li, Bangwei Gong, Bo Yang, Boji Shan, Chang Liu, Cheng Zhu, Chunhao Zhang, Congchao Guo, Da Chen, Dong Li, et al. Minimax-01: Scaling foundation models with lightning attention. *arXiv preprint arXiv:2501.08313*, 2025. 3

[28] Xingyang Li, Muyang Li, Tianle Cai, Haocheng Xi, Shuo Yang, Yujun Lin, Lvmin Zhang, Songlin Yang, Jinbo Hu, Kelly Peng, et al. Radial attention:  $o(n \log n)$  sparse attention with energy decay for long video generation. *arXiv preprint arXiv:2506.19852*, 2025. 3, 5

[29] Opher Lieber, Barak Lenz, Hofit Bata, Gal Cohen, Jhonathan Osin, Itay Dalmedigos, Erez Safahi, Shaked Meirom, Yonatan Belinkov, Shai Shalev-Shwartz, et al. Jamba: A hybrid transformer-mamba language model. *arXiv preprint arXiv:2403.19887*, 2024. 3

[30] Feng Liu, Shiwei Zhang, Xiaofeng Wang, Yujie Wei, Haonan Qiu, Yuzhong Zhao, Yingya Zhang, Qixiang Ye, and Fang Wan. Timestep embedding tells: It's time to cache for video diffusion model. In *Proceedings of the Computer Vision and Pattern Recognition Conference*, pages 7353–7363, 2025. 3

[31] Guangda Liu, Chengwei Li, Jieru Zhao, Chenqi Zhang, and Minyi Guo. Clusterkv: Manipulating llm kv cache in semantic space for recallable compression. In *2025 62nd ACM/IEEE Design Automation Conference (DAC)*, pages 1–7. IEEE, 2025. 3

[32] Xingchao Liu, Chengyue Gong, and Qiang Liu. Flow straight and fast: Learning to generate and transfer data with rectified flow. *arXiv preprint arXiv:2209.03003*, 2022. 3

[33] Cheng Lu, Yuhao Zhou, Fan Bao, Jianfei Chen, Chongxuan Li, and Jun Zhu. Dpm-solver: A fast ode solver for diffusion probabilistic model sampling in around 10 steps. *Advances in neural information processing systems*, 35:5775–5787, 2022. 3

[34] Enzhe Lu, Zhejun Jiang, Jingyuan Liu, Yulun Du, Tao Jiang, Chao Hong, Shaowei Liu, Weiran He, Enming Yuan, Yuzhi Wang, et al. Moba: Mixture of block attention for long-context llms. *arXiv preprint arXiv:2502.13189*, 2025. 1, 3

[35] Simian Luo, Yiqin Tan, Longbo Huang, Jian Li, and Hang Zhao. Latent consistency models: Synthesizing high-resolution images with few-step inference. *arXiv preprint arXiv:2310.04378*, 2023. 3

[36] Zhengyao Lv, Chenyang Si, Junhao Song, Zhenyu Yang, Yu Qiao, Ziwei Liu, and Kwan-Yee K Wong. Fastercache: Training-free video diffusion model acceleration with high quality. *arXiv preprint arXiv:2410.19355*, 2024. 3

[37] Xinyin Ma, Gongfan Fang, and Xinchao Wang. Deepcache: Accelerating diffusion models for free. In *Proceedings of the IEEE/CVF conference on computer vision and pattern recognition*, pages 15762–15772, 2024. 3

[38] Xin Ma, Yaohui Wang, Gengyun Jia, Xinyuan Chen, Ziwei Liu, Yuan-Fang Li, Cunjian Chen, and Yu Qiao. Latte: Latent diffusion transformer for video generation. *arXiv preprint arXiv:2401.03048*, 2024. 1

[39] Marcin Moczulski, Misha Denil, Jeremy Appleyard, and Nando de Freitas. Acdc: A structured efficient linear layer. *arXiv preprint arXiv:1511.05946*, 2015. 3

[40] Bo Peng, Eric Alcaide, Quentin Anthony, Alon Albalak, Samuel Arcadinho, Stella Biderman, Huanqi Cao, Xin Cheng, Michael Chung, Matteo Grella, et al. Rwkv: Reinventing rnns for the transformer era. *arXiv preprint arXiv:2305.13048*, 2023. 3

[41] Tim Salimans and Jonathan Ho. Progressive distillation for fast sampling of diffusion models. *arXiv preprint arXiv:2202.00512*, 2022. 3

[42] Jingze Shi, Yifan Wu, Yiran Peng, Bingheng Wu, Liangdong Wang, Guang Liu, and Yuyu Luo. Trainable dynamic mask sparse attention. *arXiv preprint arXiv:2508.02124*, 2025. 3

[43] Jiaming Song, Chenlin Meng, and Stefano Ermon. Denoising diffusion implicit models. *arXiv preprint arXiv:2010.02502*, 2020. 3

[44] Yang Song, Prafulla Dhariwal, Mark Chen, and Ilya Sutskever. Consistency models. 2023. 3

[45] Wenhao Sun, Rong-Cheng Tu, Yifu Ding, Zhao Jin, Jingyi Liao, Shunyu Liu, and Dacheng Tao. Vorta: Efficient video diffusion via routing sparse attention. *arXiv preprint arXiv:2505.18809*, 2025. 1, 3

[46] Ashish Vaswani, Noam Shazeer, Niki Parmar, Jakob Uszkoreit, Llion Jones, Aidan N Gomez, Łukasz Kaiser, and Illia Polosukhin. Attention is all you need. *Advances in neural information processing systems*, 30, 2017. 3

[47] Team Wan, Ang Wang, Baole Ai, Bin Wen, Chaojie Mao, Chen-Wei Xie, Di Chen, Feiwu Yu, Haiming Zhao, Jianxiao Yang, et al. Wan: Open and advanced large-scale video generative models. *arXiv preprint arXiv:2503.20314*, 2025. 1, 3, 5, 6, 2, 4

[48] Sinong Wang, Belinda Z Li, Madian Khabsa, Han Fang, and Hao Ma. Linformer: Self-attention with linear complexity. *arXiv preprint arXiv:2006.04768*, 2020. 1

[49] Guoyizhe Wei and Rama Chellappa. Vit-linearizer: Distilling quadratic knowledge into linear-time vision models. *arXiv preprint arXiv:2504.00037*, 2025. 3

[50] Jianzong Wu, Liang Hou, Haotian Yang, Xin Tao, Ye Tian, Pengfei Wan, Di Zhang, and Yunhai Tong. Vmoba: Mixture-of-block attention for video diffusion models. *arXiv preprint arXiv:2506.23858*, 2025. 1, 3, 5, 6

[51] Haocheng Xi, Shuo Yang, Yilong Zhao, Chenfeng Xu, Muyang Li, Xiuyu Li, Yujun Lin, Han Cai, Jintao Zhang, Dacheng Li, et al. Sparse videogen: Accelerating video diffusion transformers with spatial-temporal sparsity. *arXiv preprint arXiv:2502.01776*, 2025. 1, 2, 3, 5, 6

[52] Guangxuan Xiao, Yuandong Tian, Beidi Chen, Song Han, and Mike Lewis. Efficient streaming language models with attention sinks. *arXiv preprint arXiv:2309.17453*, 2023. 5

[53] Guangxuan Xiao, Jiaming Tang, Jingwei Zuo, Junxian Guo, Shang Yang, Haotian Tang, Yao Fu, and Song Han. Duoattention: Efficient long-context llm inference with retrieval and streaming heads. *arXiv preprint arXiv:2410.10819*, 2024. 3

[54] Enze Xie, Junsong Chen, Junyu Chen, Han Cai, Haotian Tang, Yujun Lin, Zhekai Zhang, Muyang Li, Ligeng Zhu, Yao Lu, et al. Sana: Efficient high-resolution image synthesis with linear diffusion transformers. *arXiv preprint arXiv:2410.10629*, 2024. 3

[55] Yunyang Xiong, Zhanpeng Zeng, Rudrasis Chakraborty, Mingxing Tan, Glenn Fung, Yin Li, and Vikas Singh. Nyströmformer: A nyström-based algorithm for approximating self-attention. In *Proceedings of the AAAI conference on artificial intelligence*, pages 14138–14148, 2021. 1

[56] Ruyi Xu, Guangxuan Xiao, Haofeng Huang, Junxian Guo, and Song Han. Xattention: Block sparse attention with an-tidiagonal scoring. *arXiv preprint arXiv:2503.16428*, 2025. 1, 3

[57] Songlin Yang, Jan Kautz, and Ali Hatamizadeh. Gated delta networks: Improving mamba2 with delta rule. *arXiv preprint arXiv:2412.06464*, 2024. 1, 3

[58] Shuo Yang, Haocheng Xi, Yilong Zhao, Muyang Li, Jintao Zhang, Han Cai, Yujun Lin, Xiuyu Li, Chenfeng Xu, Kelly Peng, et al. Sparse videogen2: Accelerate video generation with sparse attention via semantic-aware permutation. *arXiv preprint arXiv:2505.18875*, 2025. 1, 3

[59] Zhuoyi Yang, Jiayan Teng, Wendi Zheng, Ming Ding, Shiyu Huang, Jiazheng Xu, Yuanming Yang, Wenyi Hong, Xiaohan Zhang, Guanyu Feng, et al. Cogvideox: Text-to-video diffusion models with an expert transformer. *arXiv preprint arXiv:2408.06072*, 2024. 1, 5

[60] Can Yaras, Alec S Xu, Pierre Abillama, Changwoo Lee, and Laura Balzano. Monarchattention: Zero-shot conversion to fast, hardware-aware structured attention. *arXiv preprint arXiv:2505.18698*, 2025. 1, 3, 5

[61] Tianwei Yin, Michaël Gharbi, Taesung Park, Richard Zhang, Eli Shechtman, Fredo Durand, and Bill Freeman. Improved distribution matching distillation for fast image synthesis. *Advances in neural information processing systems*, 37:47455–47487, 2024. 3

[62] Tianwei Yin, Qiang Zhang, Richard Zhang, William T Freeman, Fredo Durand, Eli Shechtman, and Xun Huang. From slow bidirectional to fast autoregressive video diffusion models. In *Proceedings of the Computer Vision and Pattern Recognition Conference*, pages 22963–22974, 2025. 1

[63] Jingyang Yuan, Huazuo Gao, Damai Dai, Junyu Luo, Liang Zhao, Zhengyan Zhang, Zhenda Xie, YX Wei, Lean Wang, Zhiping Xiao, et al. Native sparse attention: Hardware-aligned and natively trainable sparse attention. *arXiv preprint arXiv:2502.11089*, 2025. 1, 3

[64] Manzil Zaheer, Guru Guruganesh, Kumar Avinava Dubey, Joshua Ainslie, Chris Alberti, Santiago Ontanon, Philip Pham, Anirudh Ravula, Qifan Wang, Li Yang, et al. Big bird: Transformers for longer sequences. *Advances in neural information processing systems*, 33:17283–17297, 2020. 3

[65] Jintao Zhang, Haofeng Huang, Pengle Zhang, Jun Zhu, Jianfei Chen, et al. Sageattention2: Efficient attention with smoothing q and per-thread quantization. In *First Workshop on Scalable Optimization for Efficient and Adaptive Foundation Models*, 2024. 3

[66] Jintao Zhang, Haoxu Wang, Kai Jiang, Shuo Yang, Kaiwen Zheng, Haocheng Xi, Ziteng Wang, Hongzhou Zhu, Min Zhao, Ion Stoica, et al. Sla: Beyond sparsity in diffusion transformers via fine-tunable sparse-linear attention. *arXiv preprint arXiv:2509.24006*, 2025. 1, 3

[67] Jintao Zhang, Jia Wei, Pengle Zhang, Xiaoming Xu, Haofeng Huang, Haoxu Wang, Kai Jiang, Jun Zhu, and Jianfei Chen. Sageattention3: Microscaling fp4 attention for inference and an exploration of 8-bit training. *arXiv preprint arXiv:2505.11594*, 2025. 3

[68] Jintao Zhang, Chendong Xiang, Haofeng Huang, Haocheng Xi, Jun Zhu, Jianfei Chen, et al. Spageattention: Accurate and training-free sparse attention accelerating any model inference. In *Forty-second International Conference on Machine Learning*, 2025. 1, 3

[69] Peiyuan Zhang, Yongqi Chen, Haofeng Huang, Will Lin, Zhengzhong Liu, Ion Stoica, Eric Xing, and Hao Zhang. Vsa: Faster video diffusion with trainable sparse attention. *arXiv preprint arXiv:2505.13389*, 2025. 1, 3, 5, 6, 7, 2, 4

# VMonarch: Efficient Video Diffusion Transformers with Structured Attention

## Supplementary Material

### A. Python code of MonarchAttention

In this section, we show the Python-like code of MonarchAttention [60] in Fig. 6.

```

def R_update(
    aR, # (m, b, d)
    cR, # (m, b)
    Kb, # (m, b, d)
    ): # Computes R, aL, cL from aR, cR
    R = softmax(bmm(aR, Kb.transpose(1, 2)) \
        / cR[:, :, None], dim=2)
    cL = sum(R * log(R), dim=2).transpose(0, 1)
    aL = bmm(R, Kb).transpose(0, 1)
    return aL, cL, R
def L_update(
    aL, # (b, m, d)
    cL, # (b, m)
    Qb, # (b, m, d)
    ): # Computes L, aR, cR from aL, cL
    L = softmax(bmm(Qb, aL.transpose(1, 2)) \
        - cL[:, None, :], dim=2)
    cR = sum(L, dim=1).transpose(0, 1)
    aR = bmm(L.transpose(1, 2), Qb).transpose(0, 1)
    return aR, cR, L
def monarch_attention(Q, K, V, m, b, T):
    # Q, K, V: (N, d), m * b = N
    # T > 0: number of steps
    Qb = Q.reshape(m, b, d).transpose(0, 1)
    Kb = K.reshape(m, b, d)
    Vb = V.reshape(m, b, d)
    aR = Q.reshape(m, b, d)
    cR = ones(m, b)

    for t in range(T):
        aL, cL, R = R_update(aR, cR, Kb)
        aR, cR, L = L_update(aL, cL, Qb)

        y = bmm(R, Vb).transpose(0, 1)
        O = bmm(L, y).transpose(0, 1)
        O = O.reshape(N, d)
    return O

```

Figure 6. Python-like code of MonarchAttention.

### B. Optimized Entropy Flash Attention

The **online softmax algorithm** computes the softmax function over a vector  $\mathbf{x} = [x_1, \dots, x_N]$  in a single pass without storing the entire vector. This is achieved by maintaining running statistics. For numerical stability, the algorithm uses the shift-invariant property of softmax with a running

maximum  $m = \max_k \{x_k\}$ . After processing  $i$  elements, it maintains a state tuple  $(m_i, S_i)$ , where  $m_i = \max_{k=1}^i \{x_k\}$  is the running maximum and  $S_i = \sum_{k=1}^i e^{x_k - m_i}$  is the denominator sum normalized by  $m_i$ . When a new element  $x_{i+1}$  arrives, the state is updated. The new maximum is  $m_{i+1} = \max(m_i, x_{i+1})$ . If the maximum changes ( $m_{i+1} > m_i$ ), the previous sum  $S_i$  must be rescaled by a factor  $\alpha = e^{m_i - m_{i+1}}$ . The general update for  $S_i$  is:

$$S_{i+1} = S_i \cdot e^{m_i - m_{i+1}} + e^{x_{i+1} - m_{i+1}} \quad (9)$$

We extend the online softmax algorithm to **online entropy**, which computes the Shannon entropy  $H(p) = -\sum p_j \log p_j$  in a single pass. The entropy can be expressed in terms of the final statistics of the online softmax:

$$H(p) = -\sum_{j=1}^N p_j \log p_j \quad (10)$$

$$= -\sum_{j=1}^N p_j ((x_j - m_N) - \log S_N) \quad (11)$$

$$= \log S_N - \frac{1}{S_N} \sum_{j=1}^N e^{x_j - m_N} (x_j - m_N) \quad (12)$$

To compute this online, we introduce a third running statistic,  $L_i$ , which is the sum of logits weighted by their unnormalized probabilities:  $L_i = \sum_{k=1}^i e^{x_k - m_i} (x_k - m_i)$ .

We now present the complete update for the state  $(m_i, S_i, L_i)$  upon receiving a new element  $x_{i+1}$ . First, find the new maximum  $m_{i+1} = \max(m_i, x_{i+1})$ .

If the maximum does not change ( $m_{i+1} = m_i$ ), the updates are additive:

$$S_{i+1} = S_i + e^{x_{i+1} - m_{i+1}} \quad (13)$$

$$L_{i+1} = L_i + e^{x_{i+1} - m_{i+1}} (x_{i+1} - m_{i+1}) \quad (14)$$

If the maximum increases ( $m_{i+1} > m_i$ ), the previous sums must be rescaled before adding the new term. Let  $\alpha = e^{m_i - m_{i+1}}$ . The updates are:

$$S_{i+1} = S_i \cdot \alpha + e^{x_{i+1} - m_{i+1}} \quad (15)$$

$$L_{i+1} = L_i \cdot \alpha + S_i \cdot \alpha \cdot (m_i - m_{i+1}) + e^{x_{i+1} - m_{i+1}} (x_{i+1} - m_{i+1}) \quad (16)$$

Noting that  $\log(\alpha) = m_i - m_{i+1}$  and letting  $p_{i+1} = e^{x_{i+1} - m_{i+1}}$ , the update for  $L_{i+1}$  can be expressed more

---

**Algorithm 2** Flash-Entropy-Attention Backward

---

**Require:**  $\mathbf{Q}, \mathbf{K}, \mathbf{V}, \mathbf{O}, \mathbf{dO} \in \mathbb{R}^{N \times d}, L, \mathbf{H}, \mathbf{dH} \in \mathbb{R}^N$ .  
**Ensure:**  $\mathbf{dQ}, \mathbf{dK}, \mathbf{dV} \in \mathbb{R}^{N \times d}$ .

- 1:  $T_r \leftarrow \lceil N/B_r \rceil, T_c \leftarrow \lceil N/B_c \rceil$ .
- 2: Compute  $D \in \mathbb{R}^N$  as  $\text{rowsum}(\mathbf{dO} \odot \mathbf{O})$ .
- 3: Initialize  $\mathbf{dQ} \leftarrow \mathbf{0}_{N \times d}$  in HBM.
- 4: **for**  $j = 1 \rightarrow T_c$  **do**
- 5:     Load  $\mathbf{K}_j, \mathbf{V}_j$  to SRAM.
- 6:     Initialize  $\mathbf{dK}_j, \mathbf{dV}_j \leftarrow \mathbf{0}_{B_c \times d}$ .
- 7:     **for**  $i = 1 \rightarrow T_r$  **do**
- 8:         Load  $\mathbf{Q}_i, \mathbf{O}_i, \mathbf{dO}_i, L_i, D_i, \mathbf{H}_i, \mathbf{dH}_i$  to SRAM.
- 9:          $\mathbf{S}_{ij} \leftarrow \mathbf{Q}_i \mathbf{K}_j^T$ .
- 10:          $\mathbf{P}_{ij} \leftarrow \exp(\mathbf{S}_{ij} - L_i)$ .
- 11:          $\mathbf{dV}_j \leftarrow \mathbf{dV}_j + \mathbf{P}_{ij}^T \mathbf{dO}_i$ .
- 12:          $\mathbf{dP}_{ij} \leftarrow \mathbf{dO}_i \mathbf{V}_j^T$ .
- 13:          $\mathbf{dS}_{ij} \leftarrow \mathbf{P}_{ij} \odot (\mathbf{dP}_{ij} - D_i)$ .  $\triangleright$  Standard Gradient
- 14:          $\mathbf{dS}_{ij} \leftarrow \mathbf{dS}_{ij} - \mathbf{dH}_i \odot \mathbf{P}_{ij} \odot (\mathbf{S}_{ij} - L_i + H_i)$
- 15:         Load  $\mathbf{dQ}_i$  from HBM.
- 16:          $\mathbf{dQ}_i \leftarrow \mathbf{dQ}_i + \mathbf{dS}_{ij} \mathbf{K}_j$ .
- 17:          $\mathbf{dK}_j \leftarrow \mathbf{dK}_j + \mathbf{dS}_{ij}^T \mathbf{Q}_i$ .
- 18:         Write  $\mathbf{dQ}_i$  to HBM.
- 19:     **end for**
- 20:     Write  $\mathbf{dK}_j, \mathbf{dV}_j$  to HBM.
- 21: **end for**

---

compactly in a form analogous to the entropy formula itself:

$$L_{i+1} = L_i \cdot \alpha + S_i \cdot \alpha \log(\alpha) + p_{i+1} \log(p_{i+1}) \quad (17)$$

After processing all  $N$  elements, the final state is  $(m_N, S_N, L_N)$ . The Shannon entropy is then calculated as:

$$H(p) = \log S_N - \frac{L_N}{S_N} \quad (18)$$

## C. Backward pass of Flash-Entropy-Attention

We provide the backward pass algorithm of FlashAttention with Online Entropy in Algorithm 2. However, the entropy term is not numerically stable; meanwhile, the gradient from entropy tends to dominate the gradient rather than the original attention output, which caused training instability. Therefore, we do not backpropagate through the entropy calculation in practice. We still provide the full backward algorithm here for completeness.

## D. Experiments details

We select Wan2.1-1.3B [47] as our primary base model for training-free and post-training experiments, while also extending our verification to the larger Wan2.1-14B model [47] and the architecturally different Wan2.2-5B model [47]. For the Wan2.1-1.3B post-training, we tune the model with a  $61 \times 448 \times 832$  input size for 1500 steps

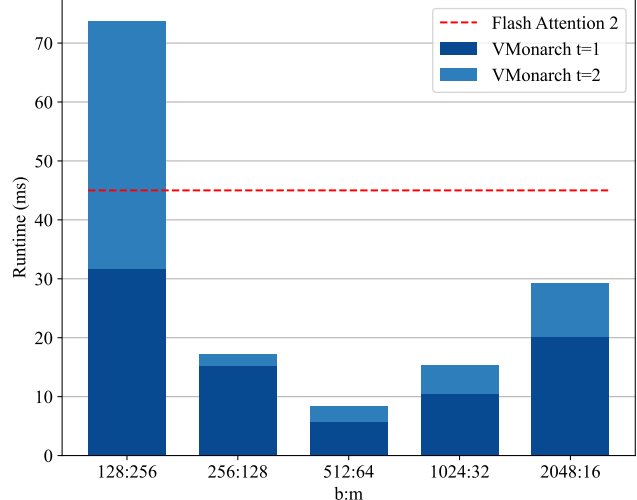


Figure A. Various computational budgets compared with FA2 at a sequence length of  $2^{15}$ . In practice,  $b$  is usually larger than 256.

on the Fastvideo Wan14B-Syn-600k dataset [69], using a learning rate of  $1 \times 10^{-6}$  and a batch size of 8. For ablation studies on this model, we fine-tune for 500 steps with the same learning rate and batch size, calculating validation loss on 32 samples split from the training dataset. Regarding the Wan2.1-14B and Wan2.2-5B models, we conduct fine-tuning on the Wan2.2-Syn-32k dataset [69] with a resolution of  $93 \times 704 \times 1280$ . To handle the increased computational load, we employ sequence parallelism with a degree of 8. Regarding the sparse attention baselines, we follow their default setting. For VSA [69], we employ a sparsity annealing schedule that gradually increases the sparsity ratio to 90%, and use its Triton version as the CUDA version is incompatible with our hardware. For VMoBA, we adopt its default cyclic partitioning strategy, alternating between 1D, 2D, and 3D attention blocks. We set the chunk sizes to 4, (7, 13), and (4, 7, 13), respectively, and use a top- $p$  (0.25) strategy for block selection for both training and inference. We test all models on VBench-Long [21] prompts with the same setting: 50 inference steps, guidance scale 5.0, and flow shift 3.0, the negative prompt is "Bright tones, overexposed, static, blurred details, subtitles, style, works, paintings, images, static, overall gray, worst quality, low quality, JPEG compression residue, ugly, incomplete, extra fingers, poorly drawn hands, poorly drawn faces, deformed, disfigured, misshapen limbs, fused fingers, still picture, messy background, three legs, many people in the background, walking backwards".

## E. Various Monarch Computation Budgets

Our kernel supports flexible attention decomposition, and its computational budget can be adjusted by varying the monarch factor sizes  $m, b$ . Theoretically, the computational complexity is minimized when  $m = b = \sqrt{N}$ , and the I/O

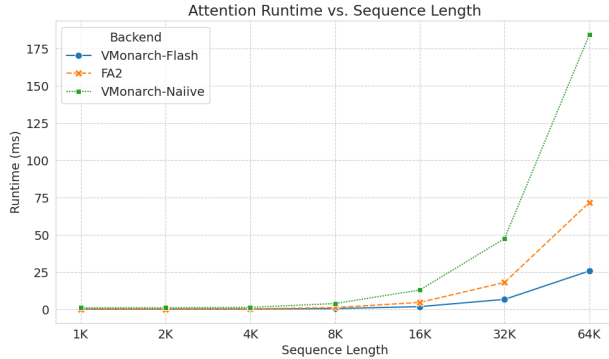


Figure 8. Speed comparison of FlashAttention2(FA2) [8], VMonarch-Naive, and our optimized VMonarch-Fast (Triton) implementation. After applying kernel optimization, VMonarch-Fast achieves an approximately  $8\times$  speedup over the naive implementation and surpasses the performance of FA2.

complexity decreases as  $b$  increases. As the I/O complexity decreases as  $m$  decreases, the best  $m$  lies in  $[1, \sqrt{N}]$ . As shown in Fig. A, we profile the kernel inference time with various computation budgets at a sequence length of 32k. In the video modality, setting  $b = 1F$  (where  $F = HW$ ) corresponds to a specific decomposition ( $b : m \approx 1024 : 32$ ), which can be further accelerated by reducing  $b$  via spatial downsampling.

## F. Kernel Optimization of VMonarch

To further enhance the efficiency of our Video Monarch Attention (VMonarch), we developed a fused kernel. We benchmark the speed of our optimized kernel against a naive PyTorch implementation. The benchmark is conducted with a batch size of 1, 12 attention heads, and a head dimension of 64. The number of iterations for VMonarch is set to 2. We test on sequence lengths ranging from  $2^{10}$  to  $2^{16}$ . The Monarch factor sizes  $m$  and  $b$  are set to  $m = 32$  and  $b = \text{sequence length}/32$ . As shown in Fig. 8, the optimized kernel provides a significant speedup, achieving approximately  $8\times$  speedup over the naive implementation and surpassing the performance of FlashAttention2 (FA2) [8].

## G. Detailed Speed and Memory Benchmarks

We benchmark the memory usage and speed of our Video Monarch Attention (VMonarch) against several baselines: Full Attention (FA2), Video Sparse Attention (VSA), and various VMoBA [50] configurations (VMoBA-1d, VMoBA-2d, VMoBA-3d, and VMoBA-3d-TopP). The comparisons are conducted on different video lengths, with results presented in Fig. 9 and Fig. 10. Our findings indicate that VMoBA encounters a significant memory overhead bottleneck at finer granularities. Furthermore, with ran-

Table 4. Similarity comparison of our and other baseline methods. All methods are evaluated under the training-free setting with a resolution of  $61 \times 448 \times 832$ .

Method	Similarity	
	PSNR $\uparrow$	SSIM $\uparrow$
FlashAttention2 (FullAttn) [8]	-	-
Video Sparse Attention (VSA) [69]	9.71	0.32
Video MoBA (VMoBA) [50]	10.61	0.30
Video Monarch (VMonarch)	12.59	0.43

dom inputs (uniform distribution), the TopP strategy used in VMoBA-3d-TopP leads to a noticeable slowdown in speed and an increase in memory consumption. We compare with FA2 as our kernel extends its Triton implementation. Our Online-Entropy Attention is also compatible with FA3, as both are based on the Online-Softmax algorithm.

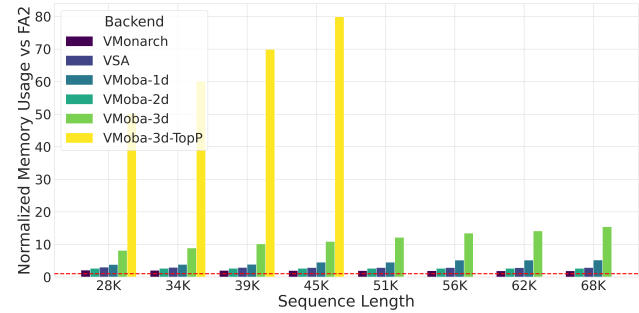


Figure 9. Memory benchmark of different attention mechanisms. We compare the relative memory usage against full attention.

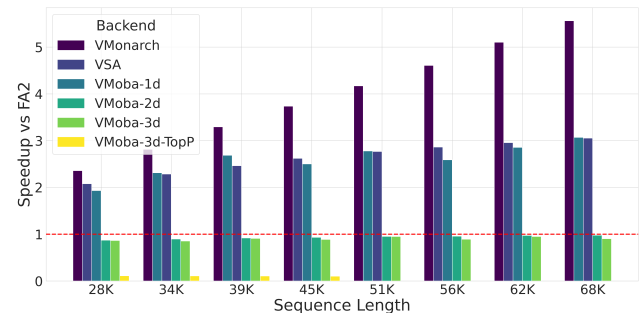


Figure 10. Speed benchmark of different attention mechanisms. We compare the relative speed against full attention.

## H. Detailed Training-free comparison

As shown in Tab. 4, VMonarch outperforms VSA and VMoBA in PSNR and SSIM under the training-free setting, demonstrating that Monarch’s block-diagonal structure effectively aligns with the spatio-temporal priors of video.

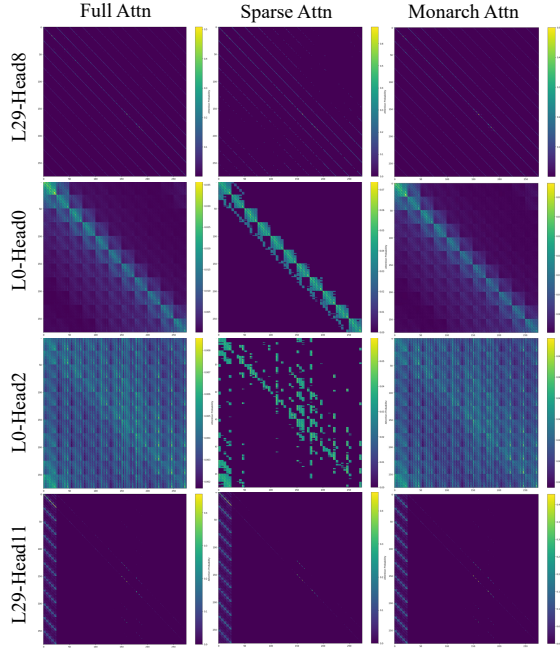


Figure 11. Attention map comparison among Full Attention, Sparse Attention, and Monarch Attention.

## I. Comparison of Attention Maps

We visualize the attention maps of Full Attention [8], Sparse Attention (corresponding to VSA [69]), and Monarch Attention (corresponding to VMonarch) of different heads on Wanx1.3B [47]. We downsample the attention maps to  $300 \times 300$  for better visualization. As shown in Fig. 11, Full Attention produces a dense attention map, while Sparse Attention generates a highly sparse attention map with many zero values. Our VMonarch does not produce an overly sparse distribution and is much more continuous compared to VSA.

## J. Manual Control of Monarch Parameters

To better understand the behavior of Monarch Attention, we conduct a detailed ablation study on its key components, with results presented in Tab. 5. We analyze the impact of the number of iterations ( $t$ ) and the manual control of the intermediate optimization terms,  $c_L$  and  $c_R$ . For  $c_L$  and  $c_R$ , we explore three strategies applied after each iteration: no control (using the updated value), fixing the value for the first frame only, and fixing the value for all frames.

Our findings reveal several key insights. First, the number of iterations is crucial; increasing from one (Exp.1, Score: 2.19) to two (Exp.8, Score: 3.29) yields a substantial performance improvement. Second, while manually controlling  $c_L$  and  $c_R$  can boost the score in the single-iteration setting (e.g., Exp.2 achieves a score of 3.11), this

benefit vanishes with two iterations. In the cases of two iterations (Exp[8-14]), none of the manual control strategies outperform the baseline. This suggests that intervening in the optimization process may disrupt the stability of the alternating updates, leading to suboptimal performance.

In contrast, our proposed recomputation mechanism (Exp.15) provides a simple yet effective solution. It achieves the highest overall score of 3.44, outperforming all manual control variants and underscoring its effectiveness in enhancing generation quality without destabilizing the core optimization.

## K. Different Monarch Factorization methods

Beyond the temporal-axis Monarch factorization method, we also explored alternative factorization strategies, such as spatial dimension factorization. Specifically, we grouped the video’s spatial dimensions  $H$  or  $W$  with a grouping unit of 4, referred to as  $(4, HWT/4)$  and  $(4, WHT/4)$  respectively. We conducted a simple comparison of different grouping methods in a zero-shot setting, with the results shown in Fig. 12. Grouping along the  $H$  or  $W$  dimensions results in significant spatial discontinuities. Additionally, we experimented with larger temporal blocks for grouping, such as dividing the sequence into four temporal segments, referred to as  $(4, THW/4)$ . We observed that this grouping method leads to substantial temporal jumps between blocks, although temporal consistency within blocks remains stable. Our default setting  $(T, HW)$  provides the best balance between spatial and temporal coherence.



Figure 12. Comparison of different Monarch factorizations.

## L. More Visual Results

We provide more visual comparisons in Fig. 13, comparing Full Attention, VSA, and our VMonarch on various prompts. The results demonstrate that VMonarch consistently produces higher-quality videos that compare favorably to Full Attention, while VSA sometimes exhibits semantic inconsistencies.

Table 5. Ablation study on VMonarch Attention. We evaluate several variants by adjusting its iterative parameters, including the number of iterations and the manual control of intermediate terms. Metrics with a superscript '1' (e.g.,  $PSNR^1$ ) are calculated on the first frame only. The score is calculated as  $Score = (PSNR + PSNR^1)/200 + (SSIM + SSIM^1)/2 + (1 - LPIPS + 1 - LPIPS^1)/2 + IQ + SC + OC$ , where IQ, SC, and OC denote Imaging Quality, Subject Consistency, and Overall Consistency, respectively. In the Method column,  $M^{(t)}$  denotes the number of iterations  $t$ . +Re represents our recomputation mechanism. For the control of  $c_R$ ,  $+c_R^*$  indicates fixing it to 1 for all frames,  $+c_R^1$  for the first frame only, and  $+c_R^0$  means no fixing. For the control of  $c_L$ ,  $+c_L^*$  indicates fixing it to the initial expected value  $\log(M)$  for all frames,  $+c_L^1$  for the first frame only, and  $+c_L^0$  means no fixing.

Exp.	Method	PSNR $\uparrow$	SSIM $\uparrow$	LPIPS $\downarrow$	PSNR $^1$ $\uparrow$	SSIM $^1$ $\uparrow$	LPIPS $^1$ $\downarrow$	IQ $\uparrow$	SC $\uparrow$	OC $\uparrow$	Score $\uparrow$
1	$M^{(1)}$	11.01	0.21	96.41%	10.21	0.12	90.44%	48.54%	87.00%	16.28%	2.19
2	$M^{(1)} + c_R^* + c_L^1$	10.66	0.23	80.39%	11.21	0.30	51.54%	62.22%	87.53%	18.85%	3.11
3	$M^{(1)} + c_R^1 + c_L^1$	10.66	0.23	80.39%	11.21	0.30	51.54%	62.22%	87.53%	18.85%	3.11
4	$M^{(1)} + c_R^1 + c_L^*$	11.01	0.18	99.78%	10.29	0.11	95.63%	41.32%	85.87%	15.69%	1.98
5	$M^{(1)} + c_R^* + c_L^*$	11.01	0.18	99.78%	10.29	0.11	95.63%	41.32%	85.87%	15.69%	1.98
6	$M^{(1)} + c_R^1 + c_L^0$	11.01	0.21	96.41%	10.21	0.12	90.44%	48.54%	87.00%	16.28%	2.19
7	$M^{(1)} + c_R^0 + c_L^1$	10.66	0.23	80.39%	11.21	0.30	51.54%	62.22%	87.53%	18.85%	3.11
8	$M^{(2)}$	11.19	0.28	52.44%	9.39	0.21	55.53%	72.17%	75.96%	19.47%	3.29
9	$M^{(2)} + c_R^* + c_L^1$	6.93	0.11	78.38%	7.90	0.16	71.14%	48.53%	97.68%	3.02%	2.42
10	$M^{(2)} + c_R^1 + c_L^1$	6.94	0.11	78.59%	7.78	0.16	71.70%	49.00%	97.88%	2.97%	2.41
11	$M^{(2)} + c_R^1 + c_L^*$	10.71	0.24	64.26%	8.68	0.12	58.73%	75.60%	90.48%	14.03%	3.12
12	$M^{(2)} + c_R^* + c_L^*$	8.12	0.17	64.85%	6.96	0.07	59.14%	52.85%	96.08%	8.66%	2.73
13	$M^{(2)} + c_R^1 + c_L^0$	11.13	0.27	55.81%	9.14	0.19	55.01%	69.62%	76.55%	19.72%	3.21
14	$M^{(2)} + c_R^0 + c_L^1$	6.51	0.13	80.88%	7.16	0.18	71.79%	49.18%	97.23%	1.51%	2.40
15	$M^{(2)} + \text{Re}$	11.55	0.29	56.96%	10.13	0.27	58.18%	73.06%	91.26%	17.19%	3.44

## M. Discussion on Monarch Attention

Monarch Attention [60] is a general form of normal self-attention with Monarch matrix [11] representation, which is suitable for sparse distribution modeling. As shown in Eq. (3), Eq. (4), Eq. (5), Eq. (6) and Eq. (7), Monarch Attention has many parameters and can derive many variants that deserve to be discussed.

**Monarch Approximation Error Analysis.** We formulate the Monarch approximation error as  $D_{KL}(S||M) \approx D_{KL}(S||M^*) + D_{KL}(M^*||M)$ . The structural error  $D_{KL}(S||M^*)$  represents the intrinsic gap between full attention  $S$  and the optimal Monarch factorization  $M^*$ , which is minimized when  $S$  aligns with block-diagonal structures; VMonarch effectively reduces this via Spatio-Temporal factorization that matches video priors. The iteration error  $D_{KL}(M^*||M)$  stems from the iterative solver, and we find that it converges after 2 iterations.

**Understanding iteration terms  $c_R$  and  $c_L$**  can be interpreted as temperature adjustment factors for the softmax function based on entropy statistics within each monarch factor  $L$  and  $R$ . They are the intermediate terms under the alternating maximization optimization process. A better optimization algorithm or a suitable optimization object target may bring simpler and more efficient intermediate terms.

**Correlation with full attention** As  $N = m \times b$ , if  $b = 1$  or  $m = 1$ , MonarchAttention reduces to standard attention. From this point of view, full attention can be viewed as a special case of Monarch attention, where only a single monarch factor is applied.

**Correlation with spatial-temporal attention** When no iteration is performed, Monarch Attention degenerates to Spatial/Temporal Attention. When only  $R$  updating Eq. (3) is applied and  $c_R$  is set to the all-ones matrix and  $L$  is set to the identity matrix, it is equal to the temporal-attention.

Although Monarch Attention [60] provides an iterative approximation algorithm to reduce  $D_{KL}(M^*||M)$ , its inefficient entropy calculation hinders scaling to long sequences. Our proposed Online-Entropy Flash Attention overcomes the OOM bottleneck via algorithm-system co-design, which is critical for the video modality. Furthermore, we leverage Spatio-Temporal Factorization aligned with video priors to directly minimize  $D_{KL}(S||M^*)$ , and introduce a general Recomputation strategy to help model convergence by losslessly approximating specific tokens.

## N. Limitations and Future Work

VMonarch has several limitations that present opportunities for future research. First, we employ a static sparsification strategy with uniform Monarch parameters across all layers and heads, whereas a dynamic strategy that adapts to the distinct distribution priors of different layers could potentially improve performance. Second, although VMonarch achieves a great theoretical sparsity, it still relies on dense attention within each Monarch factor, and sparsifying this internal computation could further boost efficiency. Third, a more balanced Monarch factorization (e.g., via spatial downsampling) could further enhance efficiency.



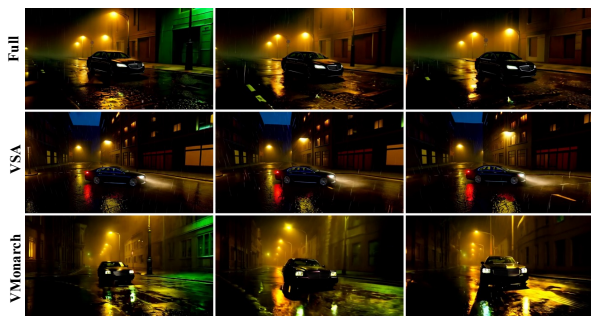
A breathtaking time-lapse captures the sun setting over a tranquil beach, where the sky transforms from a soft orange to deep purples and pinks. Whispy clouds drift gracefully across the horizon, reflecting the changing hues of the sky. The golden sun slowly dips below the water, casting a shimmering path of light on the gentle waves. Silhouettes of distant sailboats and palm trees add to the serene ambiance. As the sky darkens, stars begin to twinkle, and the last remnants of daylight fade, leaving a peaceful, starlit night over the calm, rhythmic ocean.



A joyful Corgi with a fluffy coat and perky ears bounds through a sunlit park, the golden hues of sunset casting a warm glow on the scene. The dog's playful energy is evident as it chases after a bright red ball, its short legs moving swiftly across the lush green grass. The Corgi pauses momentarily to look back at the camera, its tongue lolling out in a happy grin, before darting off again, its tail wagging furiously. The backdrop of tall trees and a serene lake reflects the soft, amber light of the setting sun, creating a picturesque and heartwarming moment.



A sleek motorcycle, gleaming under the midday sun, cruises effortlessly along a winding coastal highway. The rider, clad in a black leather jacket, helmet, and jeans, leans into the curves with precision, the ocean's azure waves crashing against rugged cliffs on either side. The engine purrs smoothly, harmonizing with the rhythmic sound of the waves. As the motorcycle glides past tall, swaying palm trees and sun-drenched sandy beaches, the horizon stretches endlessly, blending the sea's deep blue with the sea's shimmering surface. The scene captures the essence of freedom and adventure, with the coastal breeze adding a sense of exhilaration to the journey.



A sleek, black sedan glides slowly down a deserted, rain-soaked street, its headlights cutting through the misty evening air. The streetlights cast a warm, golden glow on the wet pavement, reflecting the car's silhouette as it moves. Raindrops gently patter on the car's roof and windows, creating a soothing rhythm. The surrounding buildings, with their darkened windows and muted colors, stand silent and still, adding to the serene, almost melancholic atmosphere. The car's windshield wipers sweep rhythmically, clearing the view ahead as it continues its unhurried journey through the tranquil, rain-drenched night.



A golden retriever with a shiny coat strides leisurely through a sun-dappled forest path, the morning light filtering through the trees casting a warm glow. The dog's tail wags gently as it sniffs, its ears perked up, taking in the serenity surrounding. The scene captures close-ups of its joyful expression, tongue lolling out, and eyes sparkling with contentment. As it walks, the soft crunch of leaves under its paws adds to the tranquil ambiance. The scene transitions to the dog pausing by a clear, babbling brook, lapping up the cool water, before continuing its peaceful journey through the picturesque woodland.



A serene cow with a glossy brown coat lies comfortably on a bed of fresh straw inside a rustic, sunlit barn. The gentle rays of the afternoon sun filter through the wooden slats, casting a warm, golden glow over the scene. The cow's large, expressive eyes blink slowly as it rhythmically chews its cud, creating a sense of calm and contentment. Surrounding the cow are various farm tools and bales of hay, adding to the authentic, tranquil atmosphere. The soft sounds of the barn—occasional rustling of straw and distant chirping of birds—enhance the peaceful ambiance, making it a perfect moment of rural serenity.



A sleek, black cat lounges on a sunlit poolside deck, wearing stylish, tiny sunglasses that reflect the shimmering water. The cat's fur glitters under the bright sun, and its relaxed posture exudes cool confidence. Nearby, a colorful beach towel and a half-empty glass of lemonade add to the summer vibe. The cat occasionally stretches, its sunglasses staying perfectly in place, while the gentle ripples in the pool create a soothing background. The scene captures a perfect blend of feline elegance and laid-back summer fun.



A towering Bigfoot trudges through a fierce snowstorm, its massive, fur-covered form barely visible against the swirling white. The creature's powerful strides leave deep footprints in the snow, each step echoing its immense weight and strength. Snow clings to its thick, matted fur, and its eyes, glowing faintly, peer through the blizzard with an almost human-like intensity. The wind howls around it, whipping up flurries that obscure its path, but Bigfoot moves with purpose, undeterred by the harsh elements. The scene captures the raw, untamed wilderness, with the mythical creature embodying the mystery and majesty of nature's most elusive legends.

Figure 13. More visual results comparing Full Attention, VSA, and VMonarch on various prompts.